AIChE WILEY InterScience DISCOVER SOMETHING GREAT

PARTICLE TECHNOLOGY AND FLUIDIZATION

Modeling and Measurement of Bubble Size in a Rotating Fluidized Bed

Hideya Nakamura, Tomohiro Iwasaki, and Satoru Watano
Dept. of Chemical Engineering, Osaka Prefecture University, Naka-ku, Sakai, Osaka 599-8531, Japan

DOI 10.1002/aic.11260
Published online September 13, 2007 in Wiley InterScience (www.interscience.wiley.com).

Modeling and measurement of bubble size in a rotating fluidized bed (RFB) is described. A novel model of bubble growth has been proposed based on a bubble coalescence model by Darton et al. We modified the model according to the following concepts: (i) local centrifugal acceleration and excess gas velocity are considered as the parameters in the radial direction and (ii) bubble volume flow rate locally changes depending on the radial distance. Bubbling behavior in a two-dimensional RFB was experimentally observed by means of a high-speed video camera. Bubble sizes were measured using an image analysis technique. The estimated bubble sizes by our proposed model showed good agreement with the experimental results, while the estimated values by the model for conventional fluidized bed underestimated. The bubble growth mechanism in an RFB was also discussed and then concluded that the initial bubble size decreases, and the rate of bubble growth increases with an increase in the centrifugal acceleration. © 2007 American Institute of Chemical Engineers *AIChE J,* 53: 2795–2803, 2007

Keywords: fluidization, rotating fluidized bed, bubble size, modeling, image analysis

Introduction

Fluidized bed has been widely used in many industries because of its desirable characteristics such as high heat and mass transfer rates, temperature homogeneity, easy handling, and rapid mixing of particulate materials. However, a conventional process has some limitations: it is difficult to operate under high gas velocity since the gas–solid contact becomes poor due to a generation of large bubbles, slugs, and particle entrainment; uniform fluidization of fine particles such as Geldart group-C particles[1] is also difficult due to channeling, lifting as a plug, and forming "rat holes."

Recently, a rotating fluidized bed (RFB) has gathered a special interest since it has high potential to overcome the conventional limitations. The RFB system has unique fluidization concept as shown in Figure 1. The system consists of a cylindrical plenum chamber and a cylindrical gas distributor rotating around its axis of symmetry inside the fixed plenum chamber. Because of the rotational motion of gas distributor, particles are forced to move toward the rotating vessel (gas distributor) by the centrifugal force, making annular bed near to the rotating vessel. Gas flows inward through the gas distributor, and particles are balanced by drag and centrifugal forces leading to uniform fluidization in a high centrifugal force field. This system has many advantages that: (1) it can prevent growth of large bubbles and particle entrainment even at relatively high gas velocities by controlling the vessel rotational speed[2]; (2) it imparts high centrifugal and fluid drag forces onto fine particles for uniform fluidization[3]; (3) its space requirement is very small.

The RFB has been expected to be used as some advanced industrial processes from its advantages, such as reactor of rocket propulsion in a microgravity field,[4] the high efficiency dust filter,[5,6] simultaneous removal process of NOx and soot from diesel engine exhaust gas,[7] incineration of wool scouring sludges,[8] granulation and coating of fine particles,[9–11] and handling of nanoparticles.[12,13] In spite of many published studies, a reliable RFB process has not been established yet,

Correspondence concerning this article should be addressed to S. Watano at watano@chemeng.osakafu-u.ac.jp.

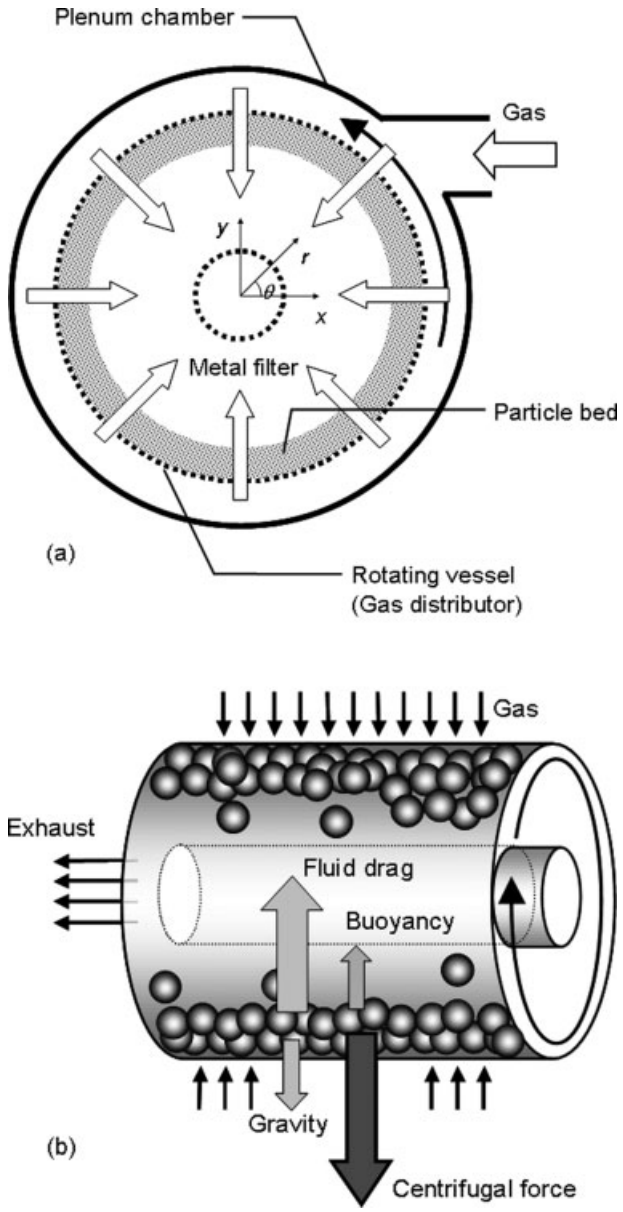

Figure 1. RFB system: (a) front view and (b) over view.

because the fundamental fluidization mechanism has not been well studied.

There are a few reports of fundamental fluidization mechanism in an RFB. So far, Fan et al.,[14] Chen,[15] and Kao et al.[16] have reported the modeling of bed pressure drop based on the conservation equations of mass and momentum balance in the radial direction. Chen[15] proposed the layer-by-layer fluidization model, in which the fluidization of particle bed can take place from the surface to the outside of particle bed. Shi et al.[17] has experimentally investigated the heat transfer between particle and gas phase. They finally proposed the empirical correlation which predicted the heat transfer coefficients. The particle mixing has been investigated by Kroger et al.[18] and Qian et al.[19] However, they only reported the effect of gas velocity on the particle mixing, never mentioned the effect of other operating parameters. Takahashi et al.[20] has just reported the empirical correlation for prediction of the coefficient of lateral particle dispersion under various operating parameters. Recently, fluidization behavior of fine particles has been reported by Matsuda et al.[12] and Quevedo et al.[13] They analyzed the fluidization behavior of nano-agglomerates and proposed the model of the agglomerate size in a high-centrifugal force field. The studies of numerical modeling have also been reported based on CFD[21,22] and DEM-CFD coupling model.[23]

It is well known that bubbling characteristics in a conventional fluidized bed greatly influence the fundamental fluidization phenomenon, such as gas–solid contact, particle mixing, entrainment, and so on.[24] Bubbling characteristics thus become the critical parameters for design and control of fluidized bed process. However, no reports have been made regard to the bubbling characteristics of RFB. Or the existing models for conventional fluidized bed have been directly used by substituting centrifugal acceleration for gravity term.[12] Only Chevray et al.[25] has reported the mathematical model of bubble dynamics such as velocity and trajectory by the Lagrangian approach. However, there was no experimental data evaluating the validity of their model.

The overall objective of this study is to theoretically analyze the bubbling characteristics in an RFB. The bubble size, which is one of the most important bubble characteristics, was mainly analyzed. A mathematical model for predicting the bubble growth was proposed. Validity of the proposed model was evaluated by comparing the bubble size actually measured by an image analysis technique in a two-dimensional RFB with the estimated values by our proposed model and the available model for a conventional fluidized bed.

Modeling of Bubble Growth in an RFB

So far, many studies have been conducted for the prediction of bubble growth in a conventional fluidized bed. Darton et al.[26] has proposed a mathematical model of bubble growth for Geldart's group B and D particles based on the staged coalescence model, which assuming that bubble growth occurred in the stage between adjacent two bubbles. According to this model, bubble diameter D_b can be expressed as follows:

$$D_b = \frac{0.54(u_0 - u_{mf})^{0.4}\left(z + 4.0\sqrt{A_c}\right)^{0.8}}{g^{0.2}} \quad (1)$$

where u_0, u_{mf}, z, and A_c are superficial gas velocity, minimum fluidization gas velocity, height above gas distributor, and area of distributor per hole, respectively.

However, available models for conventional fluidized bed cannot be directly applied to RFB, because the fluidization mechanisms are totally different. Figure 2 shows the schematic diagram of fluidization state in an RFB. The gas velocities and centrifugal acceleration locally change in an RFB, although they are independent from bed height in a conventional fluidized bed. In this study, we modified the bubble growth model proposed by Darton et al.[26] based on this differences. The two concepts of modeling are as follows: (i) centrifugal acceleration and excess gas velocity are consid-

ered as a function of radial distance from the surface of gas distributor L; and (ii) bubble volume flow rate passing through the bed as bubbles increases with an increase in L.

According to Darton et al.,[26] the bubble coalescence is assumed to occur in stages as shown in Figure 3. The distance L_N from the surface of the gas distributor at the Nth stage of coalescence can be assumed as the following equation[26]:

$$L_N = \lambda D_{c0} + \lambda D_{c1} + \cdots + \lambda D_{c(N-1)} \tag{2}$$

where D_c is the circle equivalent diameter of A_c ($A_c = 0.25\pi D_c^2$). λ shows the bubble coalescence constant. Diameter of bubble at the perforated distributor can also be estimated by the following equation[27]:

$$D_b = 1.38\left[\frac{u-u_{mf}}{g^{0.5}}A_c\right]^{0.4}. \tag{3}$$

Therefore, the correlation between the D_c and D_b at the Nth stage of coalescence can be expressed as follows:

$$D_{cN} = 0.75\frac{g_N'^{0.25}D_{bN}^{1.25}}{(u-u_{mf})_N^{0.5}} \tag{4}$$

where g_N' and $(u - u_{mf})_N$ are the local centrifugal acceleration and local excess gas velocity at L_N, respectively. g_N' and $(u - u_{mf})_N$ are considered as a function of L, as expressed[16]:

$$g_N' = \frac{G_0 g}{\beta_N} \tag{5}$$

$$(u-u_{mf})_N = \beta_N \cdot u_0 - \frac{1}{\beta_N}\frac{\mu}{\rho_f d_p}\left[\left(33.7^2 + 0.0408\frac{\rho_f(\rho_p-\rho_f)d_p^3 G_0 g}{\mu^2\beta_N}\right)^{0.5} - 33.7\right] \tag{6}$$

where G_0 is a dimensionless centrifugal factor, which is defined as a ratio of the centrifugal acceleration at the surface of rotating gas distributor to the gravitational acceleration ($g = 9.8$ m/s^2) as shown in the Eq. 7:

$$G_0 = \frac{R_V\omega^2}{g} \tag{7}$$

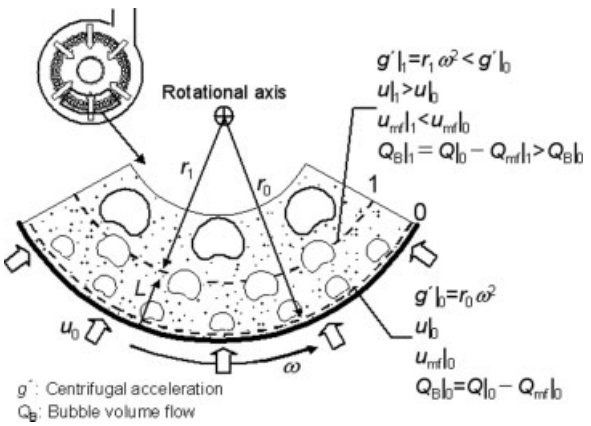

Figure 2. Fluidization state in RFB.

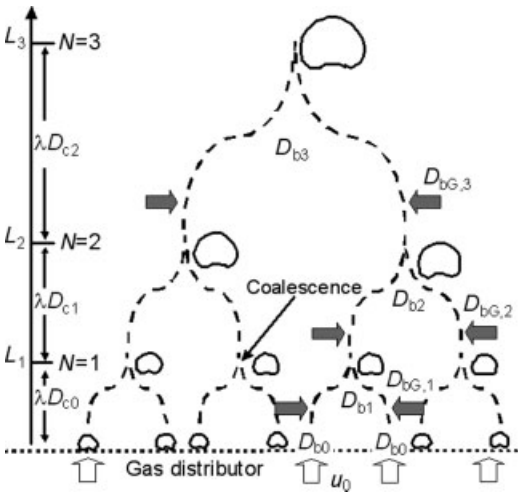

Figure 3. Schematic diagram of bubble growth model in RFB.

where R_V and ω are radius and angular velocity of the rotating vessel. β in Eqs. 5 and 6 also indicates the dimensionless radius defined as:

$$\beta_N = \frac{R_V}{(R_V - L_N)} \tag{8}$$

The volume balance of bubble in each coalescence stage can be expressed as follows:

$$\left.\begin{aligned} D_{b1}^3 &= 2D_{b0}^3 + 2D_{bG,1}^3 \\ D_{b2}^3 &= 2D_{b1}^3 + 2D_{bG,2}^3 \\ D_{b3}^3 &= 2D_{b2}^3 + 2D_{bG,3}^3 \\ \vdots \quad &\quad \vdots \quad \quad \vdots \\ D_{b(N-1)}^3 &= 2D_{b(N-2)}^3 + 2D_{bG,(N-1)}^3 \end{aligned}\right\} \tag{9}$$

where, $D_{bG,N}$ is defined as the "gained bubble diameter" at Nth coalescence stage due to the increased bubble volume flow rate, since the excess gas velocity increases with an increase in L. It is defined as:

$$D_{bG,N} = 1.38\left[\frac{(u-u_{mf})_N - (u-u_{mf})_{(N-1)}}{g_{(N-1)}'^{0.5}}A_{c(N-1)}\right]^{0.4}. \tag{10}$$

Finally, the correlation between the bubble diameter and the dimensionless radius can be obtained by numerically solving the above equations. Figure 4 shows an algorithm for bubble size calculation. In this study, D_{b0} for the gas distributor of the sintered mesh was calculated by the following equation[27]:

$$D_{b0} = 3.77\frac{(u-u_{mf})_{L=0}^2}{G_0 g}. \tag{11}$$

The value of λ was preliminarily determined as 0.77 which gave the smallest sum-of-squares error between experimental and estimated results at the operating parameter ($G_0 = 10$ and $(u - u_{mf})_{L=0} = 0.11$ m/s), which were arbitrary chosen.

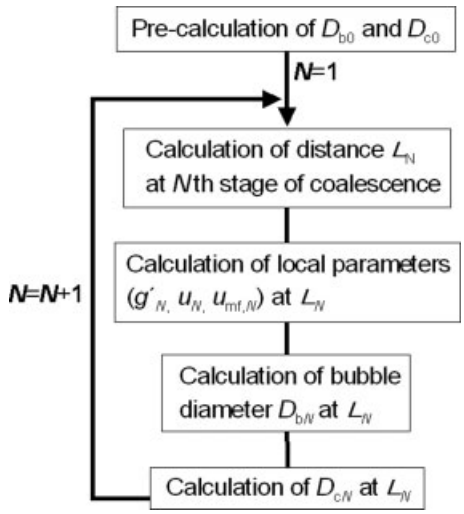

Figure 4. Schematic flow of algorithm for bubble size calculation.

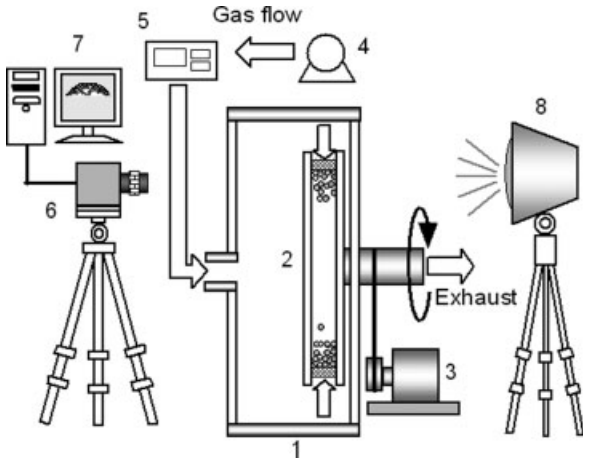

Figure 5. Experimental setup.

1, Plenum chamber; 2, rotating vessel (gas distributor; I.D. 250 mm × D. 5 mm); 3, motor; 4, blower; 5, mass flow meter; 6, high-speed video camera; 7, data analysis system; 8, metal halide lamp.

Darton et al.[26] fitted λ based on the literature data for conventional fluidized bed, and $\lambda = 1.17$ was chosen. λ in an RFB (=0.77) showed smaller value than that in a conventional fluidized bed (=1.17). In this model, smaller λ means that coalescence of bubbles more easily occurred. We believe that the difference of λ comes from the geometry of vessel in an RFB: with an increase in a distance from vessel, radius of curvature increases in an RFB. Two bubbles can get closer to each other in this case, and accordingly bubble coalescence can easily occur, although the value of λ might be constant in relatively large vessel size. We have already started to analyze the effect of vessel geometry on the constant λ, and the details will be reported in our subsequent article.

Experimental

Experimental apparatus

Figure 5 shows the experimental setup for visualization of bubbling behavior in the RFB. A thin porous cylindrical plate (I.D. 250 mm × D. 5 mm), which was made of stainless sintered mesh with 20 μm openings, was used as rotating gas distributor. The covers of the chamber and rotating vessel are both made of transparent acrylic plastic that allows observation of bubbling behavior at various circumferential locations. Spherical glass beads (FUJISTONE GB-01, Fujirika industrial) were used as experimental model particles and their median diameter and density were 136 μm and 2520 kg/m^3, respectively. The particles of 170.0 g were charged into the vessel of which the initial bed height was 31 mm. The bubbling behavior in the two-dimensional RFB was observed by means of a high-speed video camera (FASTCAM MAX, Photoron). The recording frame rate and shutter speed were set at 3000–4000 frames/s and 0.14 ms, respectively. A metal halide lamp was used as light source, which was set at backside of the particle bed. Figure 6 shows the representative recorded images of the bubbling behavior at four different positions. The digitized recorded images consisted of 512 × 256 picture elements (pixel). The whole visualized area was 16 cm × 8 cm, which corresponded to 0.16 mm × 0.16 mm of spatial resolution per one pixel.

In this study, bubbling behavior was observed in the range between $G_0 = 10$ and 40 (267–534 rpm). We could not analyze the bubbling behavior at the small rotational speed lower than $G_0 = 5$, because particles could not make a uniform annular bed due to downward gravitational force. The experiment at higher G_0 was also impossible because of the limitation of our experimental system.

Image analysis

The image analysis techniques were used for the measurement of bubble size. The analysis procedures were as follows: The first step was the binarization for segmentation of

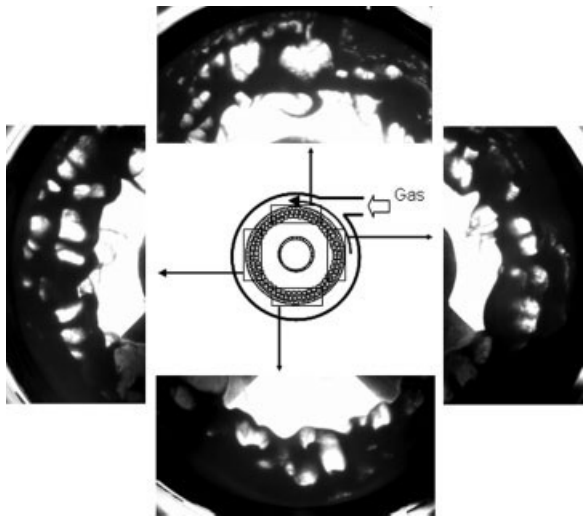

Figure 6. Visualized bubbling behavior in RFB; $G_0 = 20$, $(u - u_{mf})_{L=0} = 0.170$ m/s.

bubbles from the emulsion phase (background). A typical recorded image of a bubble and its gray level histogram are indicated in Figures 7a,b, respectively. The histogram was normally bimodal and the two peaks were separated obviously, provided that the image contrast was sufficient. The peak at a low gray level corresponded to the emulsion phase, whereas the other corresponded to the bubble phase. These two phases were distinguished by the optimum threshold value which was determined based on the discriminant analysis method.[28] In this method, the degree of thresholding $\eta(T)$ of each gray level T was calculated by the following equation:

$$\eta(T) = \frac{\sigma_B^2(T)}{\sigma_w^2(T)} \tag{12}$$

where $\sigma_B^2(T)$ and $\sigma_w^2(T)$ are interclass and intraclass variances of pixels, respectively. These were defined as the following equations:

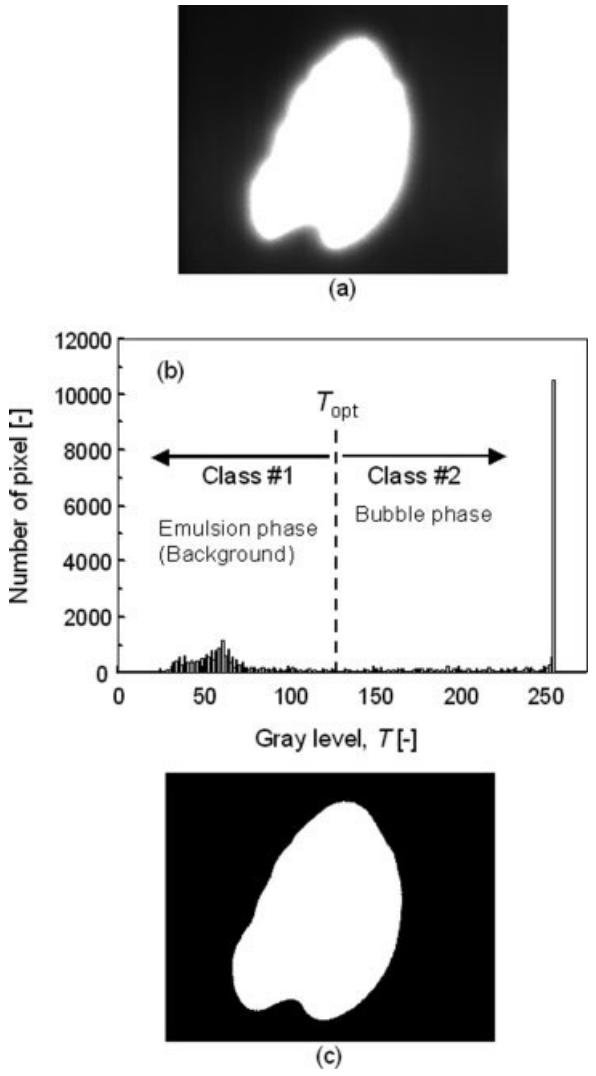

Figure 7. Example of segmentation of bubble phase: (a) original recorded image; (b) gray level histogram of; (c) binarized image.

$$\sigma_w^2(T) = f_1\sigma_1^2 + f_2\sigma_2^2 = \frac{1}{N_P}\left[\sum_{i=0}^{T-1}\left(i-\overline{T}_1\right)^2 n_i + \sum_{i=T}^{255}\left(i-\overline{T}_2\right)^2 n_i\right] \tag{13}$$

$$\sigma_B^2(T) = f_1\left(\overline{T_1}-\overline{T}\right)^2 + f_2\left(\overline{T_2}-\overline{T}\right)^2 = \frac{1}{N_P}\left[\sum_{i=0}^{T-1}\left(\overline{T_1}-\overline{T}\right)^2 n_i + \sum_{i=T}^{255}\left(\overline{T_2}-\overline{T}\right)^2 n_i\right] \tag{14}$$

where, f_1, σ_1, $\overline{T_1}$ are the normalized number of pixels, variance, averaged gray level within $0 \le i \le T-1$ (class #1 in Figure 7b), respectively. f_2, σ_2, $\overline{T_2}$ also indicate those of within $T \le i \le 255$ (class #2 in Figure 7b), respectively. n_i, N_P, $\overline{T}$ show the number of pixels at each gray level, total number of pixels, total average of gray level. The optimum threshold value (T_{opt}) can be obtained when the $\eta(T)$ takes the maximum value. Figure 7c shows the binarized image based on this method. This binarization processing was individually applied to the measured bubbles. In the second step, individual bubble diameter $D_{b,i}$ was calculated as an equivalent diameter of sphere according to the following equation:

$$D_{b,i} = \left(\frac{6}{\pi}A_{b,i}H\right)^{1/3} \tag{15}$$

where $A_{b,i}$ is the white projected area of individual bubble in the binarized image, and H is the bed thickness. The position of the bubble can also be calculated as the center of gravity of the white projected area. Finally, the volume averaged bubble diameter $\overline{D_b}$ was calculated by the following equation:

$$\overline{D_b} = \left(\frac{6}{\pi}\overline{V_b}\right)^{1/3} \tag{16}$$

where $\overline{V_b}$, which is the averaged volume of bubble in the range of certain β to $\beta + \Delta\beta$, was obtained by the following equation:

$$\overline{V_b} = \frac{\pi}{6}\int_0^\infty D_b^3\phi(D_b)dD_b \tag{17}$$

where $\phi(D_b)dD_b$ show the number fraction of bubble within the range of D_b to $D_b + \Delta D_b$. The total numbers of the measured bubble were almost 600 at every operating condition.

The bubble sizes in a conventional fluidized bed were preliminarily measured in order to evaluate the validity of the analysis method. A two-dimensional fluidized bed, of which the dimensions were H. 450 mm $\times$ W. 150 mm $\times$ D. 5 mm, was used as the experimental apparatus. The sintered mesh with 100 μm openings was used as the gas distributor. Spherical glass beads, which are the same one used in the RFB experiment, were also used as powder samples. The particles of 400.0 g were charged and the initial bed height was set at 19 cm. Brightness (histogram of gray level) and spatial resolution per one pixel was the same as those in the case of RFB.

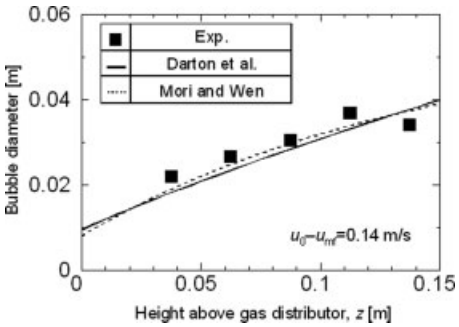

Figure 8. Measured bubble size in two-dimensional conventional fluidized bed.

Figure 8 shows the averaged bubble diameters as a function of its height above the gas distributor. Solid line shows the estimated bubble diameter by the correlation of Darton et al.[26] Dotted line also indicates the estimated values by the correlation of Mori and Wen.[29] This correlation was expressed as the following equations;

$$\frac{D_{\mathrm{bm}} - D_{\mathrm{b}}}{D_{\mathrm{bm}} - D_{\mathrm{b0}}} = \exp(-0.30z/D_{\mathrm{t}}) \tag{18}$$

$$D_{\mathrm{bm}} = 2.59g^{-0.2}[(u_0 - u_{\mathrm{mf}})A_{\mathrm{t}}]^{0.4} \tag{19}$$

As seen in Figure 8, the measured bubble diameters showed good agreement with the estimated results by Darton et al.[26] and Mori–Wen.[29] It is thus confirmed the analysis method here is suitable for bubble size measurement.

Results and Discussion

Comparison between the experimental and estimated results of bubble size

Figure 9 shows an example of averaged bubble diameter in the RFB as a function of dimensionless radius, β. Dotted curve shows the predicted value by the model for conventional fluidized bed expressed as the Eq. 1.[26] Here, centrifugal acceleration at the surface of the gas distributor ($9.8 \cdot G_0$) was directly substituted for gravity term (g) in the Eq. 1. Solid curve is the estimated result by our proposed model. Bubble diameters increased with an increase in β due to the bubble growth. Our model could estimate bubble diameters with a higher accuracy than the predicted ones by the model for conventional fluidized bed. Figures 10 and 11 compared between the experimental and the estimated bubble diameters by our model and the model for conventional fluidized bed at various operating parameters. The predicted bubble diameter by our model showed good agreement with the experimental ones even if the operating parameters changed, while the model for conventional fluidized bed underestimated the experimental results by −50% deviation. Some errors were still observed in Figure 10 in the range of low bubble diameter. This is because the small bubbles could not be visualized accurately because of the limit of the vessel depth. In other words, the bubble which was sufficiently larger than vessel depth could only be observed. We thus believe that the actual bubble diameter in lower range become smaller than the experimental one.

Bubble growth mechanism in an RFB

The bubble growth mechanism in an RFB was discussed based on our proposed model. Figure 12 shows simulation results of bubble diameter as a function of distance from the distributor. The excess gas velocity at gas inlet was 0.17 m/s in each case. The bubble size in the RFB became much smaller than that in the conventional fluidized bed, which was calculated by the Eq. 1. The bubble diameter also decreased when G_0 increased from 10 to 40. However,

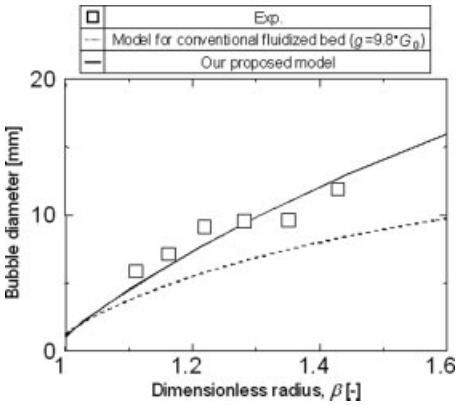

Figure 9. Bubble diameter as a function of dimensionless radius; G_0 = 10 (267 rpm), $(u - u_{\mathrm{mf}})_{L=0}$ = 0.17 m/s.

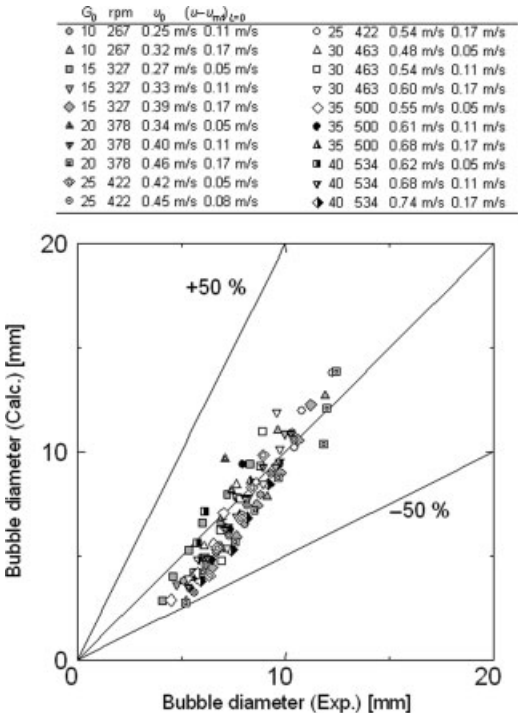

Figure 10. Comparison between experimental and estimated bubble diameters by our proposed model.

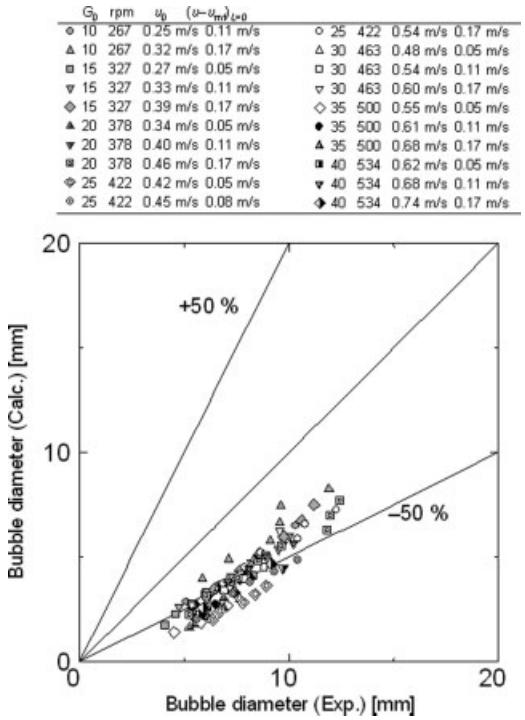

Figure 11. Comparison between experimental and estimated bubble diameters by the model for conventional fluidized bed.

bubble diameter reversely increased when G_0 increased further from 40, although the initial bubble size slightly decreased. The dimensionless bubble diameters, which were normalized by the initial bubble diameter, are shown in Figure 13 as a function of dimensionless radius β. The dimensionless bubble diameter more rapidly increased at higher G_0. It means that the rate of bubble growth increases with an increase in G_0. Figure 14 shows the local bubble Froude number Fr_b at different G_0. It can be defined as:

$$Fr_b = \frac{(u - u_{mf})_\beta}{\sqrt{\left(\frac{R_v}{\beta}\right) g'}} \tag{20}$$

Fr_b means the ratio of inertial force caused by bubble movement to the local centrifugal force at a certain β. With an

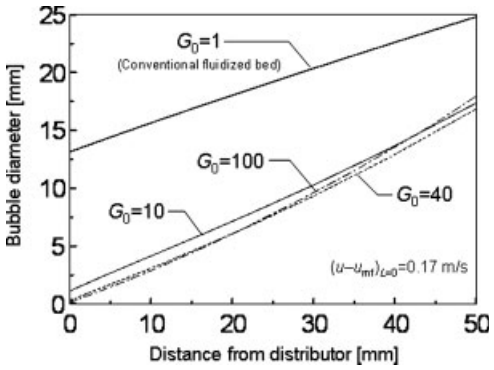

Figure 12. Theoretical curves of bubble diameter as a function of distance from distributor.

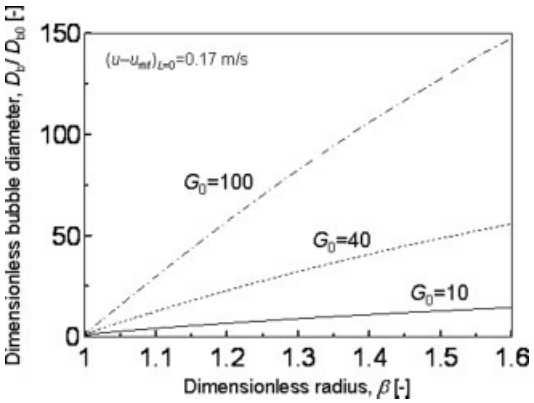

Figure 13. Dimensionless bubble diameters at different G_0.

Bubble diameters were normalized by the initial bubble size.

increase in β, Fr_b increased in each G_0, since the excess gas velocity increases and the centrifugal force decreases with an increase in the distance from the vessel wall. It should be noted that the slope of the curve increased with an increase in G_0. The rate of increase in Fr_b corresponds to the driving force of the bubble growth due to the gained bubble as indicated by the Eq. 10. The rate of bubble growth thus became higher with an increase in G_0. Figure 15 indicates the schematic illustration of the bubble size change at different centrifugal accelerations. Consequently, the mechanism of bubble growth in an RFB can be considered as the initial bubble size decreases and the rate of bubble growth increases with an increase in G_0.

Conclusions

Modeling and measurement of bubble growth in a two-dimensional RFB were conducted. The estimated bubble size by our proposed model showed good agreement with the experimentally measured ones, while the predicted ones by the existing model for conventional fluidized bed underestimated the experimental results by −50%. The validity of our following concepts used in the modeling of bubble growth were thus confirmed: (i) the terms of acceleration and excess gas velocity are considered as the parameters in the radial

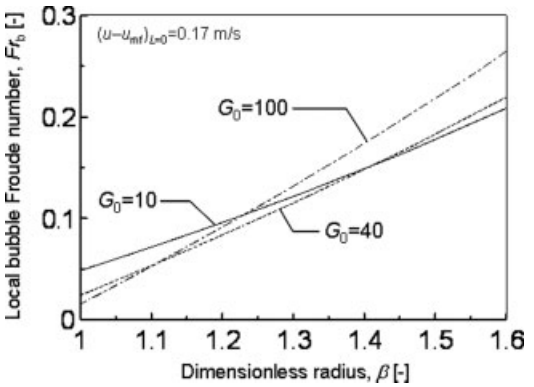

Figure 14. Local bubble Froude number at different G_0.

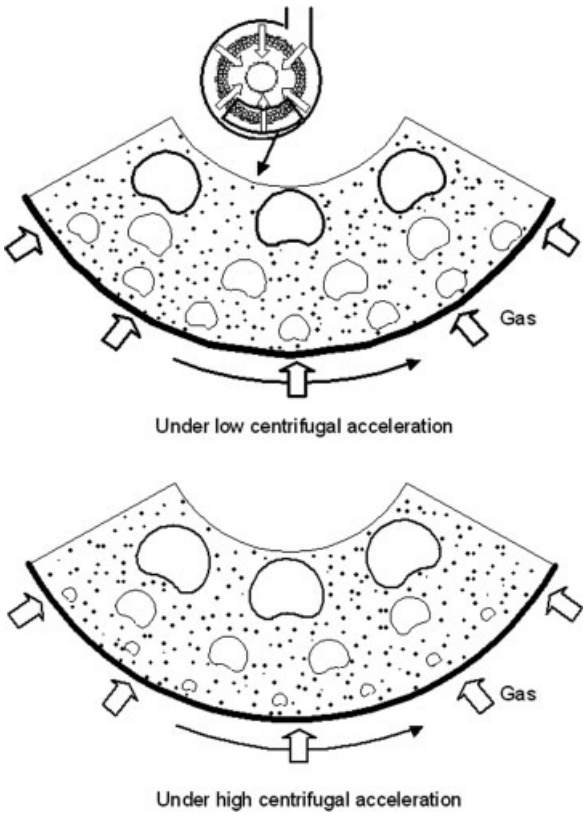

Figure 15. Change in bubble size at different centrifugal acceleration.

direction, and (ii) bubble volume flow rate increases with an increase in a radial distance from the surface of rotating gas distributor. Accordingly, the obtained results concluded the bubble growth mechanism as the initial bubble size decreases and the rate of bubble growth increases with an increase in centrifugal acceleration.

On the basis of our new insights, it is expected to provide further details of the fundamental fluidization phenomenon in an RFB such as heat and mass transfer, particle mixing, and so on.

Acknowledgments

Authors acknowledge the financial support by the Grant-in-Aids for JSPS Research Fellow (No. 7233) from the Ministry of Education, Science, Sports, and Culture of Japan.

Notation

A_b = area of white projected bubble image, m^2
A_c = area of distributor per hole, m^2
A_t = cross-sectional area of bed, m^2
D_c = circle equivalent diameter of A_c, m
D_b = equivalent spherical bubble diameter, m
D_{b0} = initial bubble diameter, m
D_{bG} = gained bubble diameter, m
d_p = particle diameter, m
D_t = diameter of bed, m
G_0 = dimensionless centrifugal factor, nondimensional
g = gravitational acceleration = 9.8 m/s^2
g' = local centrifugal acceleration, m/s^2
f = normalized number of pixels, dimensionless
Fr_b = bubble froude number, dimensionless
H = bed thickness, m
L = radial distance from rotating gas distributor, m
n_i = number of pixels at each gray level, dimensionless
N_P = total number of pixels, dimensionless
Q_B = bubble volume flow rate, m^3/s
R_V = radius of vessel, m
T = gray level, dimensionless
T_{opt} = optimum gray level for binarization, dimensionless
u = superficial gas velocity, m/s
u_0 = superficial gas velocity at gas inlet, m/s
u_{mf} = minimum fluidization velocity, m/s
$\overline{V_b}$ = averaged bubble volume, m^3
z = height above gas distributor, m

Greek letters

β = dimensionless radius, nondimensional
η = degree of thresholding, dimensionless
λ = constant in Eq. 2, nondimensional
μ = gas viscosity, Pa s
ρ_f = gas density, kg/m^3
ρ_p = particle density, kg/m^3
σ_B = interclass variance of pixel, dimensionless
σ_W = intraclass variance of pixel, dimensionless
ω = angular velocity of rotating vessel, rad/s

Subscript

N = sequential number of bubble coalescence

Literature Cited

1. Geldart D. Types of gas fluidization. *Powder Technol*. 1973;7:285–292.
2. Nakamura H, Watano S. Numerical simulation of particle fluidization behaviors in a rotating fluidized bed. *Stud Surf Sci Catal*. 2006;159:505–508.
3. Qian GH, Bágyi I, Burdick IW, Pfeffer R, Shaw H, Steves JG. Gas–solid fluidization in a centrifugal field. *AIChE J*. 2001;47:1022–1034.
4. Ludewig H, Manning AJ, Raseman CJ. Feasibility of rotating fluidized bed reactor for rocket propulsion. *J Spacecraft*. 1974;11:65–71.
5. Pfeffer R, Gabriel I, Tardos GI, Gal E. The use of a rotating fluidized bed as a high efficiency dust filter. In: Ostergaard K, Sorensen A, editors. *Fluidization V*. New York: American Institute of Chemical Engineering, 1986:667–674.
6. Qian GH, Burdick IW, Pfeffer R, Shaw H, Steves JG. Soot removal from diesel engine exhaust using a rotating fluidized bed filter. *Adv Environ Res*. 2004;8:387–395.
7. Tsutsumi A, Ju W, Yoshida K. Reduction of NO in diesel exhaust by soot using a centrifugal fluidized bed. *AIChE Symp Ser*. 1996;92:86–90.
8. Wong WY, Lu Y, Nasserzadeh VS, Swithenbank J, Shaw T, Madden M. Experimental investigation into the incineration of wool scouring sludges in a novel rotating fluidized bed. *J Hazard Mat* B. 2000;73:143–160.
9. Watano S, Imada Y, Hamada K, Wakamatu Y, Tanabe Y, Dave RN, Pfeffer R. Microgranulation of fine powders by a novel rotating fluidized bed granulator. *Powder Technol*. 2003;131:250–255.
10. Watano S, Nakmura H, Tanabe Y, Iwamoto D, Hamada K. Wet coating onto fine cohesive pharmaceutical powders by an innovative rotating fluidized bed. *Powder Hand Process*. 2003;15:390–394.
11. Watano S, Nakamura H, Hamada K, Wakamatu Y, Tanabe Y, Dave RN, Pfeffer R. Fine particle coating by a novel rotating fluidized bed coater. *Powder Technol*. 2004;141:172–176.
12. Matsuda S, Hatano H, Kuramoto K, Tsutsumi A. Modeling for size reduction of agglomerates in nanoparticle fluidization. *AIChE J*. 2004;50:2763–2771.
13. Quevedo J, Pfeffer R, Shen Y, Dave RN, Nakamura H, Watano S. Fluidization of nano agglomerates in a rotating fluidized bed. *AIChE J*. 2006;52:2401–2412.

14. Fan LT, Chang CC, Yu YS, Takahashi T, Tanaka Z. Incipient fluidization condition for a centrifugal fluidized bed. *AIChE J*. 1985;31: 999–1009.
15. Chen YM. Fundamentals of a centrifugal fluidized bed. *AIChE J*. 1987;33:722–728.
16. Kao J, Pfeffer R, Tardos GI. On partial fluidization in a rotating fluidized bed. *AIChE J*. 1987;33:858–861.
17. Shi MH, Wang H, Hao YL. Experimental investigation of the heat and mass transfer in a centrifugal bed dryer. *Chem Eng J*. 2000; 78:107–113.
18. Kroger DG, Abdelnour G, Levy EK, Chen JC. Particle distribution and mixing in a centrifugal fluidized bed. In: Grace JR, Matsen JM, editors. *Fluidization*. New York: Plenum Press, 1980:349–356.
19. Qian GH, Bágyi I, Pfeffer R, Shaw H, Steves JG. Particle mixing in rotating fluidized beds: inferences about the fluidized state. *AIChE J*. 1999;45:1401–1410.
20. Takahashi T, Kaseno S, Komoto M, Shibata S. Lateral solid particles in a centrifugal fluidized bed. *J Chem Eng Japan*. 1988;21: 493–497.
21. Zhu C, Lin CH, Qian GH, Pfeffer R. Modeling of the pressure drop and flow field in a rotating fluidized bed. *Chem Eng Commun*. 2003;190:1132–1154.
22. Ahmadzadeh A, Arastoopour H, Teymour F, Numerical simulation of gas and particle flow in a rotating fluidized bed. *Ind Eng Chem Res*. 2003;42:2627–2633.
23. Nakamura H, Watano S, Numerical modeling of particle fluidization behavior in a rotating fluidized bed. *Powder Technol*. 2007;171:106–117.
24. Kunii D, Levenspiel O. *Fluidization Engineering*, 2nd ed. Boston: Butterworth-Heinemann, 1991:137.
25. Chevray R, Chan YNI, Hill FB. Dynamics of bubbles and entrained particles in the rotating fluidized bed. *AIChE J*. 1980;26:390–398.
26. Darton RC, Lanauze RD, Davidson JF, Harrison D. Bubble growth due to coalescence in fluidized bed. *Trans IChemE*. 1977;55:274–280.
27. Miwa T, Mori S, Kato T, Muchi I. Behavior of bubbles in gaseous fluidized bed. *Kagaku Kougaku*. 1971;35:770–776.
28. Watano S, Miyanami K. Image processing for on-ling monitoring of granule size distribution and shape in fluidized bed granulation. *Powder Technol*. 1995;83:55–60.
29. Mori S, Wen CY. Estimation of bubble diameter in gaseous fluidized bed. *AIChE J*. 1975;21:109–115.

Manuscript received Feb. 16, 2007, and revision received May 9, 2007.